Dalton Transactions

ROYAL SOCIETY OF CHEMISTRY

PAPER

View Article Online
View Journal | View Issue

Cite this: *Dalton Trans.*, 2025, **54**, 15808

Inverse effect of a covalently attached electron–proton transfer mediator in the oxygen reduction reaction

Anjila I. Siddiqui, Sanyam, Rupesh Nain, Anirban Mondal * and Biswajit Mondal *

Received 26th May 2025,
Accepted 18th September 2025

DOI: 10.1039/d5dt01227a

rsc.li/dalton

In this work, the electron–proton transfer mediator (EPTM) BQ/H_2Q was covalently attached to the salophen ligand (Sal-H_2Q), and the ORR activity of its iron complex Fe(Sal-H_2Q) was compared with that of the salophen complex of iron without the EPTM, using acetic acid as the external proton source in acetonitrile. The rate of the ORR was found to be much higher for Fe(Sal), giving a peak current of 222 μA, while for Fe(Sal-H_2Q), it was 115 μA at a similar potential. Selectivity measurements revealed that both catalysts show selective water formation. This observation holds for other solvent systems as well. The findings in this study are contrary to the general observation that the covalent attachment of BQ/H_2Q EPTM enhances the ORR reactivity.

1. Introduction

The oxygen reduction reaction (ORR) is pivotal in fuel cell technology, in which oxygen is reduced at the cathode. The ORR is a multi-proton/multi-electron process, and the product selectivity varies depending on the degree of reduction. While the reduction of oxygen to water is thermodynamically favorable, its reduction to hydrogen peroxide is kinetically accessible (eqn (1) and (2)).[1]

$$O_2 + 2H^+ + 2e^- \rightarrow H_2O_2 \quad E^\circ = 0.695\ \text{V } \textit{vs.}\ \text{SHE} \qquad (1)$$

$$O_2 + 4H^+ + 4e^- \rightarrow 2H_2O_2 \quad E^\circ = 1.229\ \text{V } \textit{vs.}\ \text{SHE} \qquad (2)$$

For practical applications of the ORR, water formation is the desired process. Thus, significant efforts have been made to design catalysts with preferential ORR selectivity towards water formation.[2–4] Installing proton relays, H-bonding residues, and covalent attachment of electron–proton transfer mediators (EPTM) are among the many strategies for achieving a high percentage of H_2O during the ORR.[5–9] Recently, benzoquinone/hydroquinone (BQ/H_2Q) has emerged as a promising EPTM for efficient ORR. In one study, the redox mediator BQ/H_2Q was used in combination with Co–salophen for the ORR, and the synergy between them directed the reaction towards selective water formation with an enhanced rate.[10] A polydentate cobalt complex with a covalently attached quinol group was investigated, and its selectivity towards water was found to be driven by the presence of the redox-active quinol.[11] Various iron complexes with attached quinol groups were also found to be effective in enhancing the activity and selectivity towards water in the ORR.[12,13] In our earlier report, we also attached the redox mediator BQ/H_2Q covalently in the salophen ligand framework and studied its effect on rate and selectivity using its cobalt complex.[14] The catalyst Co(Sal-H_2Q), in which the BQ/H_2Q redox mediator was covalently attached, outperformed its analogue Co(Sal), in which no redox-active mediator was attached, in terms of water selectivity and was found to furnish 80% water while Co(Sal) yielded only 3% water under homogenous non-aqueous conditions. The observed activity is associated with the H_2Q unit, which helped in O–O bond breakage through the delivery of electrons and protons. Thus, H_2Q has gained significant attention as a covalently attached redox mediator in the ORR literature. In the context of this strategy, however, changing the metal center to Fe has been scarcely investigated. Verifying the function of hydroquinone mediators with ligand systems that contain Fe as the central metal ion is crucial, because Fe is frequently utilized as a catalyst for the ORR and oxygen activation process.[15–20]

In this study, we have explored the salophen ligand system using iron as the metal center to study the effect of changing the metal on ORR activity when the BQ/H_2Q EPTM is covalently attached ([Fe(III)(Sal)]Cl, abbreviated as Fe(Sal), and [Fe(III)(Sal-H_2Q)]Cl, abbreviated as Fe(Sal-H_2Q)) (Scheme 1). To our surprise, we found that the ORR rate for Fe(Sal) is much higher than that of Fe(Sal-H_2Q); however, the catalysts Fe(Sal-H_2Q) and Fe(Sal) both show preferential selectivity toward

Department of Chemistry, IIT Gandhinagar, Palaj, Gujarat-382355, India.
E-mail: mondal.biswajit@iitgn.ac.in

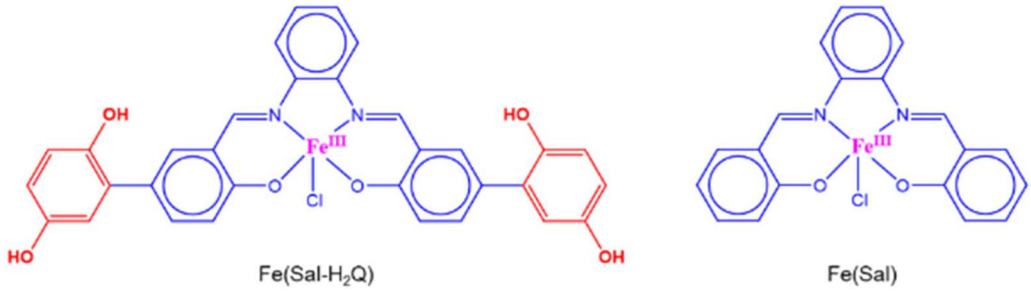

Scheme 1 Catalysts used in this study.

water formation in the ORR. This observation is true across different solvent systems. This study differs from past literature utilizing EPTMs for the ORR, as the presence of the H_2Q group in the Fe(III) complex here resulted in a decrease in ORR activity. Thus, it emphasizes the inverse effect of covalently attached H_2Q on the ORR rate or reactivity. A DFT study was performed to obtain insights into the energy steps associated with the ORR pathway for both catalysts.

2. Results and discussion

ORR in a non-aqueous medium

The ligands (Sal) and (Sal-H_2Q) were synthesized using the reported literature procedures.[21,22] The ligands were characterized *via* NMR (Fig. S1c and d) and UV-visible spectroscopy (Fig. S2). The Fe(III)Cl(L) complexes of the ligands Fe(Sal-H_2Q) and Fe(Sal) were synthesized by metallation with anhydrous $FeCl_3$ in ethanol. Both the complexes in Scheme 1 were characterized using mass spectrometry Fe(Sal) calc m/z – 370.0405, found – 370.0403, Fe(Sal-H_2Q) calc m/z – 586.0827, found – 586.0804 (Fig. S1a and b) and UV-visible spectroscopy (Fig. S3), along with molar extinction coefficients (Table S1). The complexes and ligands were also characterized by FT-IR (Fig. 2c). Cyclic voltammetry (CV) of Fe(Sal) in acetonitrile in 300 mM acid under nitrogen (N_2) revealed a peak at −0.58 V *vs.* $Fc^{+/0}$, corresponding to Fe(III/II). CV of Fe(Sal-H_2Q) under the same electrochemical conditions shows two redox events, one reversible redox event at −0.59 V assigned to Fe(III/II) and another quasi-reversible redox event with an anodic peak potential (E_{pa}) of −0.26 V and cathodic peak potential (E_{pc}) of −0.31 V for the BQ/H_2Q couple (Fig. 1a and b, inset). Voltammograms recorded at different scan rates under nitrogen-purged conditions without external acid showed that plotting the peak current of Fe(III/II) *vs.* the square root of the scan rate produces a linear dependence for both the complexes, suggesting the redox process to be diffusion-controlled (Fig. S4a–d). The redox event for Fe(Sal) at −0.67 V *vs.* $Fc^{+/0}$ for Fe(III/II) (Fig. S4b) in the absence of acid matches well with one report in the literature, in which a Fe(salophen) complex was utilized for CO_2 reduction in acetonitrile and a Fe(III/II) redox event was found at −0.69 V *vs.* $Fc^{+/0}$.[23] This confirmed the electrochemical characterization of the complex. For Fe(Sal-H_2Q), the Fe(III/II) redox event was recorded at −0.68 V *vs.* $Fc^{+/0}$, while the E_{pc} for the BQ/H_2Q couple was found at −0.36 V in the absence of acetic acid (Fig. S4a). This shows that the redox event centered at −0.68 V corresponds to the metal-centered redox event. For the electrochemical ORR, when the system is purged with oxygen (O_2) in the presence of 300 mM acid, for Fe(Sal), the reversibility of the Fe(III/II) redox process vanishes, and a large

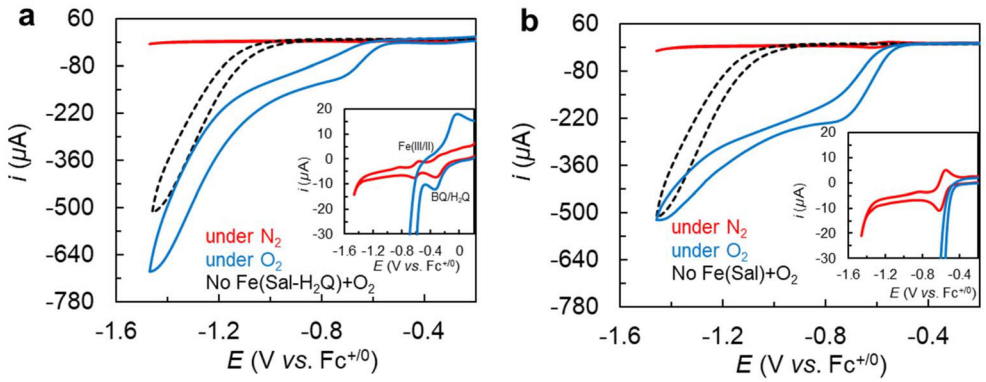

Fig. 1 Cyclic voltammograms of (a) Fe(Sal-H_2Q) and (b) Fe(Sal) under N_2 (red trace) and O_2 (blue trace). Conditions: 0.5 mM each of (Sal-H_2Q), and Fe(Sal), 300 mM AcOH, 0.1 M Bu_4NBF_4, acetonitrile. Working electrode: glassy carbon, reference electrode: Ag/AgCl, counter electrode: Pt wire, scan rate = 50 mV s^{-1}. Grey trace: blank glassy carbon under O_2.

catalytic current coinciding with the Fe(III/II) process due to the ORR is observed. The onset of the ORR appeared at −0.42 V for Fe(Sal) and −0.48 V for Fe(Sal-H_2Q) with catalytic peak currents of 222 μA and 115 μA, respectively (Fig. 1a and b). The ORR peak current observed for Fe(Sal) was higher than that for Fe(Sal-H_2Q). A control experiment with the free ligand (Sal-H_2Q) shows that the ORR by Fe(Sal-H_2Q) involves a metal-centred redox event under the experimental conditions and does not originate from the H_2Q unit, as the ORR by the free ligand coincides with that of the blank GCE ORR, which has an onset of around −0.97 V *vs.* $Fc^{+/0}$, while the onset for the ORR with the metal complex Fe(Sal-H_2Q) was observed at −0.48 V (Fig. S5). In the presence of a lower acid concentration of 30 mM, the ORR activity was also higher for Fe(Sal), with a peak current of 161 μA compared to Fe(Sal-H_2Q), which had a peak current of 35 μA (Fig. S6). Thus, Fe(Sal-H_2Q), in which the EPTM is covalently attached, showed an inverse effect in terms of ORR activity compared to earlier reported Co variants. However, there is an increase in activity in terms of the peak current for Fe(Sal) as well as Fe(Sal-H_2Q) when BQ is added externally. Here, the increment is greater for Fe(Sal) than for Fe(Sal-H_2Q) (Fig. S7a and b). This shows that the activity of Fe(Sal-H_2Q), even in the presence of externally added BQ, is inferior to that of Fe(Sal). Thus, whether the mediator is covalently attached or added externally, Fe(Sal) was found to perform better compared to Fe(Sal-H_2Q). The ORR activity was also checked under buffered conditions. In the presence of 50 mM acid and 50 mM Bu_4NOAc, the catalytic onset potential shifted cathodically with a decrease in peak current owing to the stronger binding of acetate as a ligand, as previously reported.[13] Fe(Sal) still produced a higher current compared to Fe(Sal-H_2Q) during the ORR under buffered conditions (Fig. S8). To check whether the solvent played any role in the observed activity, the ORR was also carried out in DMF, but changing the solvent did not cause a change in the catalytic behavior. The same trend was observed in DMF with both 30 mM and 300 mM acid concentrations (Fig. S9a and b).

A kinetic study was carried out to determine the rate law with respect to the catalyst, proton, and O_2 concentration. A linear dependence was found for the catalyst concentration, O_2 concentration, and acid concentration for both catalysts, suggesting first-order kinetics with respect to each of them (Fig. S10–S12).

The higher ORR current for Fe(Sal) may result from either a higher catalytic rate or better selectivity of the ORR toward water. To understand this further, the product selectivity in the ORR was analyzed *via* a spectrophotometric method using $Ti(O)SO_4$ with decamethylferrocene as a chemical reductant (Fig. S13). $Ti(O)SO_4$ forms a complex with H_2O_2, producing absorbance at 421 nm, as can be seen in the calibration plot at various concentrations (Fig. S14); however, no increase in the absorbance at 421 nm was observed after adding $Ti(O)SO_4$ for either of the catalysts, indicating that no H_2O_2 was formed. This suggests that both catalysts are selective towards the formation of water in the ORR. A similar trend was observed during selectivity studies using RRDE in a non-aqueous medium (Fig. S15). Both the catalysts were found to be selective towards water formation with n values of 3.9 for Fe(Sal) and 3.6 for Fe(Sal-H_2Q) (Table S2, calculated using eqn (4), *vide infra*). Thus, the higher ORR current for Fe(Sal) suggests a higher catalytic rate for the ORR in comparison to Fe(Sal-H_2Q).

To gain insight into the resting state of the Fe(Sal-H_2Q) catalyst, FT-IR and CV experiments were performed. The redox process of pure benzoquinone under nitrogen-saturated conditions in acetonitrile consists of two reversible redox events at −0.81 V and −1.38 V *vs.* $Fc^{+/0}$ in the absence of acid, corresponding to the simultaneous one-electron reduction of benzoquinone to a radical anion and dianion, respectively. However, the process becomes quasi-reversible in the presence of excess acid, featuring a two-electron and two-proton process with cathodic peak potential of −0.64 V. This is related to the reduction of benzoquinone to hydroquinone, as has been reported.[24] This can be observed through calculating the charge under the shaded area in the CV of benzoquinone in the absence and presence of 300 mM acetic acid (Fig. 2a). In the absence of acid, the charge under the shaded area for the process at −0.81 V was found to be 2.23×10^{-4} C, while that for the process at −1.38 V was 1.77×10^{-4} C. The similar amount of charge for both events indicates the involvement of an equal number of electrons (one electron each). In the presence of 300 mM acid, the charge passed was found to be 4.63×10^{-4} C for the process at −0.64 V, which is almost double that observed in the absence of acid. Comparing the magnitude of charge passed, it can be concluded that the redox event occurring at −0.64 V is a two-electron process and leads to the formation of hydroquinone. Similar calculations were done for Fe(Sal-H_2Q) in the presence of 300 mM acid under nitrogen-saturated conditions (Fig. 2b). The charge passed under the shaded portion at −0.59 V was found to be 1.28×10^{-6} C, corresponding to the one-electron reduction of Fe(III) to Fe(II), while for the BQ/H_2Q couple at a cathodic peak potential of −0.31 V, the charge was 5.34×10^{-6} C, indicating the involvement of a total of four electrons, corresponding to the redox of the two hydroquinone units covalently attached to the salophen ligand. The results show that in the presence of excess acid, the reduction of benzoquinone is a two-electron and two-proton process forming hydroquinone. The same was found in the case of Fe(Sal-H_2Q). In FT-IR, the peak at around 1600 cm^{-1} corresponds to the imine C=N bond present in the free ligands and their metal complexes, while a broad peak above 3000 cm^{-1} was observed for pure hydroquinone, corresponding to hydroxyl groups; this peak was also present in the free ligand Sal-H_2Q as well as its metalated complex Fe(Sal-H_2Q) (Fig. 2c). However, this peak was absent in the free ligand Sal and its metalated complex Fe(Sal). This suggests that in the resting state of Fe(Sal-H_2Q), the quinone remains in the hydroquinone state.

A plot of $E_{1/2}$ *vs.* the log of acid concentration for Fe(III/II) and the BQ/H_2Q redox couple in Fe(Sal-H_2Q) under N_2 saturation yields slopes of 58.4 and 54.8 mV dec^{-1}, respectively, while the value is 62.3 mV dec^{-1} for Fe(III/II) in Fe(Sal), confirming a Nernstian process (Fig. 3a and b). When $E_{cat/2}$ is

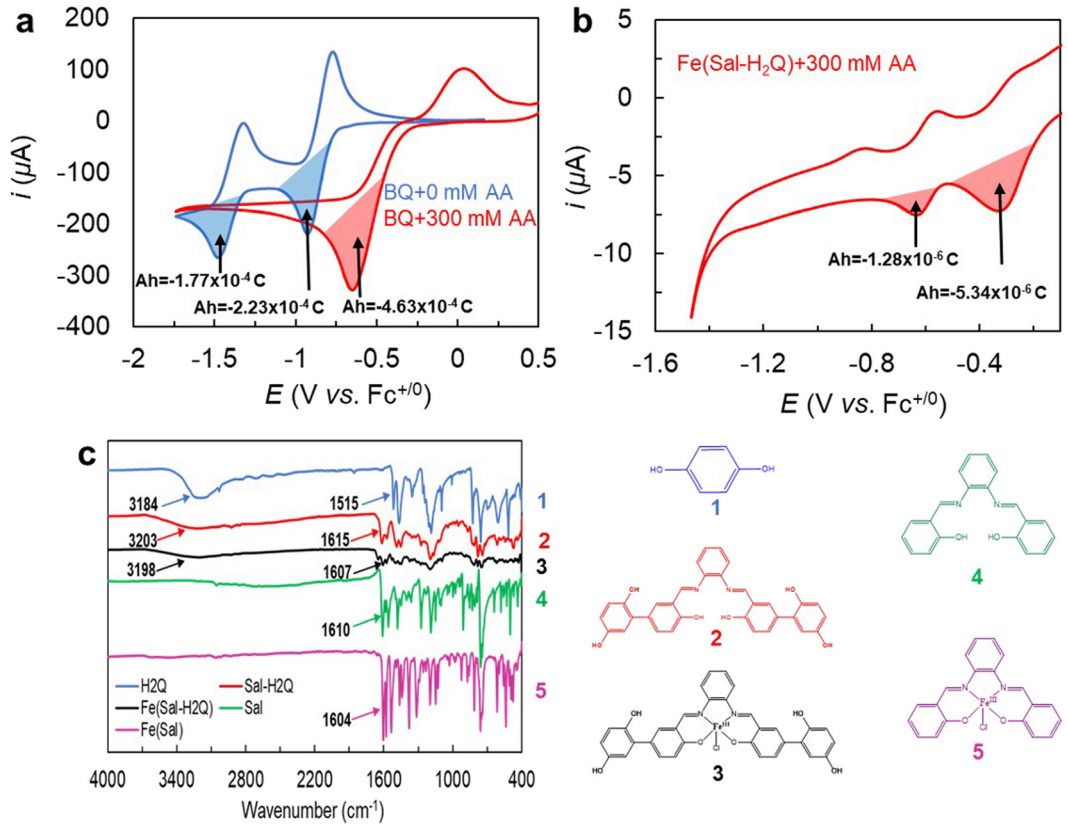

Fig. 2 Cyclic voltammograms of (a) 10 mM BQ in the absence (blue) and presence (red) of 300 mM AcOH and (b) 0.5 mM Fe(Sal-H_2Q) in 300 mM AcOH under N_2 in acetonitrile. Conditions: working electrode: glassy carbon, reference electrode: Ag/AgCl, counter electrode: Pt wire, 0.1 M Bu_4NBF_4. Scan rate = 50 mV s^{-1}, (c) FT-IR spectra of pure hydroquinone (1), Sal-H_2Q (2), Fe(Sal-H_2Q) (3), Sal (4), and Fe(Sal) (5).

plotted against the log of the acid concentration, Fe(Sal-H_2Q) yields a steeper slope compared to Fe(Sal) (Fig. 3c). The Fe(II) readily binds with O_2, and the ORR coincides with the Fe(III/II) redox couple. $E_{cat/2}$ shows significant acid dependence. Taken together, these suggest a proton-coupled electron transfer to Fe(III)–$O_2^{\bullet-}$ as the potential-determining step.

k_{obs} was determined using the peak-current method for both catalysts (Fig. S16 and S17). It was calculated using the following equation:[25]

$$\frac{i_c}{i_p} = \frac{n_c}{0.4463}\sqrt{\frac{RTk_{obs}}{F\upsilon}} \quad (3)$$

where i_c = catalytic current, i_p = current for Fe(III/II); n_c = 4 (O_2 to H_2O), R = universal gas constant = 8.314 J K^{-1} mol^{-1}, T = 300 K, F = 96 500 C mol^{-1}, υ = scan rate (V s^{-1}).

It was found that the value of k_{obs} was higher for Fe(Sal) (86 s^{-1}) compared to Fe(Sal-H_2Q) (40 s^{-1}), indicating a higher ORR rate for Fe(Sal). The overpotential was calculated using OCP measurements in the presence of 300 mM acetic acid in acetonitrile and was calculated to be 1.05 V *vs.* $Fc^{+/0}$ for Fe(Sal) and 1.06 V *vs.* $Fc^{+/0}$ for Fe(Sal-H_2Q) (Fig. S18).

ORR in an aqueous medium

Reactivity testing in an aqueous medium is crucial for evaluating the practical applications of any ORR catalyst. The selectivity of the catalysts in the current study was also examined in an aqueous medium using rotating ring disk electrochemistry (RRDE) at pH 4 and 5. The number of electrons transferred to oxygen (n) was calculated using the following equation:

$$n = 4 \times \frac{i_D}{i_D + (i_R/N)} \quad (4)$$

where n is the number of electrons transferred per molecule of O_2, i_D is the disk current, i_R is the ring current, and N is the collection efficiency of the platinum ring (15%).

Both catalysts are insoluble in water, and hence, inks of the catalysts were prepared in DCM and drop-casted on a glassy carbon disk electrode. The ORR was tested at pH 4 and pH 5. The cyclic voltammogram of Fe(Sal-H_2Q) in pH 4 under nitrogen conditions shows two anodic redox events, one at 0.77 V *vs.* NHE corresponding to the BQ/H_2Q couple and another at −0.03 V for Fe(III/II), while the cathodic redox events for BQ/H_2Q and Fe(III/II) merged to give a single redox event at −0.24 V. Fe(Sal) displays one quasi-reversible redox event with an anodic peak potential at 0.38 V and cathodic peak potential at

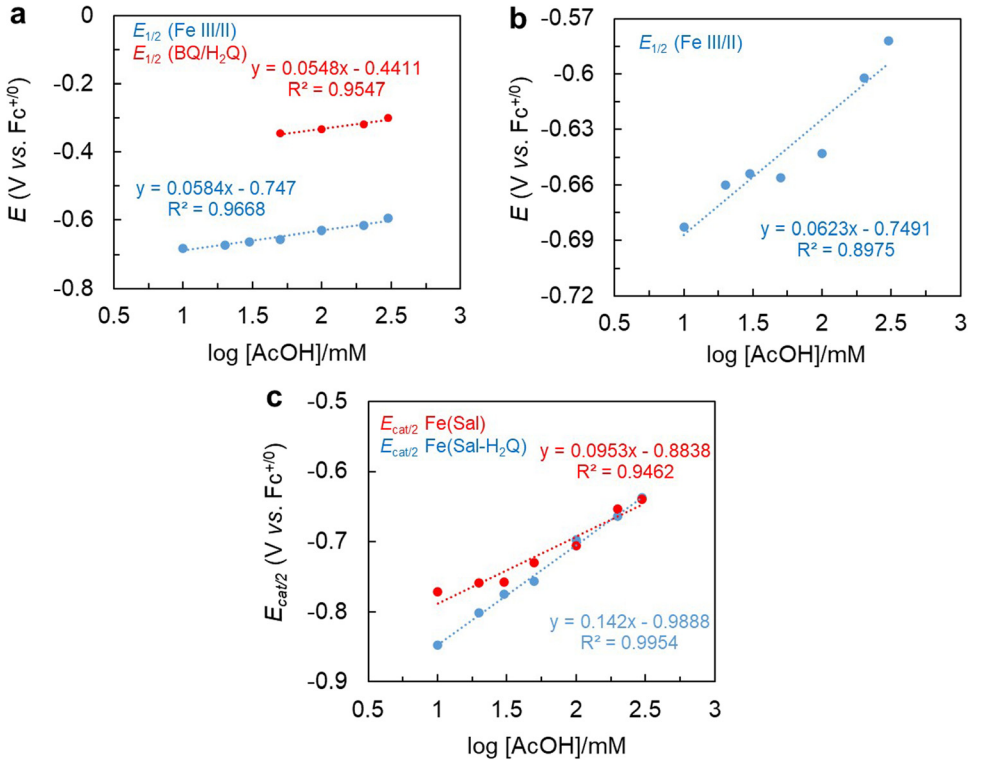

Fig. 3 Plots of (a) the $E_{1/2}$ of the Fe(III/II) and BQ/H_2Q couple against the log of the concentration of acid for Fe(Sal-H_2Q), (b) the dependence of the $E_{1/2}$ of the Fe(III/II) couple on the log of the concentration of acid for Fe(Sal) under N_2, and (c) dependence of the $E_{cat/2}$ on the log of concentration of acid for both catalysts. Conditions: 0.5 mM of each catalyst, 0.1 M Bu_4NBF_4, acetonitrile. Working electrode: glassy carbon, reference electrode: Ag/AgCl, counter electrode: Pt wire, scan rate = 50 mV s^{-1}.

−0.10 V (Fig. 4a and b). The scan rate dependence plot for both the catalysts at pH 4 shows a linear curve when the peak current is plotted against the scan rate, indicating that the electrochemical process is adsorption-controlled (Fig. S19a–d). The UV-Vis data for Fe(Sal) in water (neutral pH) and at pH 5 are similar, which suggests that the complex is stable under the experimental conditions (Fig. S20). While performing RRDE, the ring potential was held at 0.73 V to oxidize all the H_2O_2 generated during the experiment. The RRDE data at 300 rpm at both pH values show a greater ORR current for Fe(Sal) as compared to Fe(Sal-H_2Q) and are consistent with the data obtained in a non-aqueous medium. The RRDE data revealed that both complexes show preferential ORR selectivity toward water (Fig. 4c and d) and are congruent with the data obtained for homogeneous non-aqueous ORR, the non-aqueous RRDE data, and with the computational analysis (Fig. 5 and Table 1).

Computational details

In this study, we performed thermodynamic calculations to investigate the catalytic pathways for two iron-based catalysts: one with a hydroquinone substituent, Fe(Sal-H_2Q), and one without it, Fe(Sal). Our objective was to evaluate the Gibbs free energy changes (ΔG) associated with crucial reaction intermediates, thereby assessing the thermodynamic favorability of producing two distinct products from the oxygen reduction reaction: hydrogen peroxide (H_2O_2) and water (H_2O). All quantum mechanical calculations were performed using Gaussian 09, with GaussView for visualization.[26] We optimized the ground-state geometries of the catalysts using density functional theory (DFT) with the B3LYP functional and the 6-31G (d,p) basis set.[27] Single-point frequency calculations were performed on each optimized structure to determine the thermodynamic parameters, including Gibbs free energies for the formation pathways of both H_2O_2 and H_2O. The Solvation Model based on Density (SMD) was employed using the parameters for Acetonitrile (ACN) as the implicit solvent. The dielectric constant (ε) of acetonitrile used in the SMD model is $\varepsilon = 37.5$, consistent with standard values implemented in Gaussian.

The thermodynamic results provide crucial insights into the selectivity and efficiency of Fe(Sal) and Fe(Sal-H_2Q) as catalysts for the oxygen reduction reaction (ORR). Both pathways, *i.e.*, those leading to the formation of H_2O or H_2O_2, are thermodynamically feasible, as indicated by the negative Gibbs free energy changes (ΔG) for the reactions under both catalytic conditions (Fig. 5). However, a clear preference for water formation is observed, with the ΔG values for H_2O formation being consistently more negative than those for H_2O_2 formation. This thermodynamic preference underscores the inherent favorability of H_2O as the final product in these systems. Transition state calculations were also carried out for both H_2O and H_2O_2 formation (Fig. S21). It was observed that the activation barriers were significantly higher for H_2O_2 formation compared to H_2O

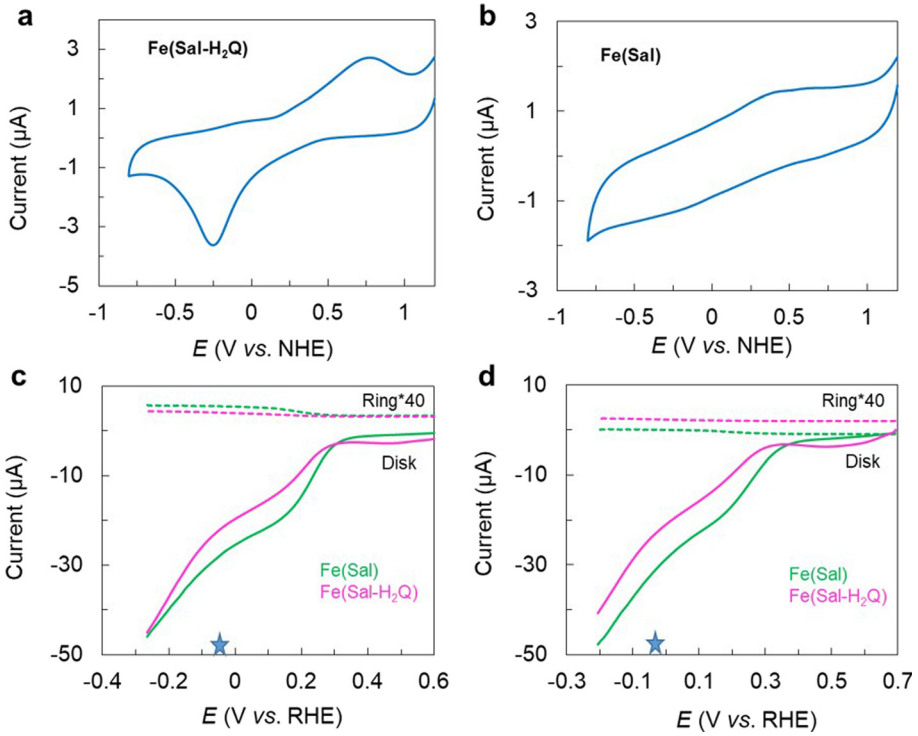

Fig. 4 Cyclic voltammograms of (a) Fe(Sal-H_2Q) and (b) Fe(Sal) under N_2 at pH 4. Conditions: working electrode: glassy carbon, reference electrode: Ag/AgCl, counter electrode: Pt wire, scan rate = 50 mV s^{-1}. RRDE plots for Fe(Sal) in green and Fe(Sal-H_2Q) in pink, in air-saturated solutions of (c) pH 4 and (d) pH 5 at 300 rpm. Conditions: disk electrode: glassy carbon, ring: platinum held at 0.73 V, scan rate = 50 mV s^{-1}.

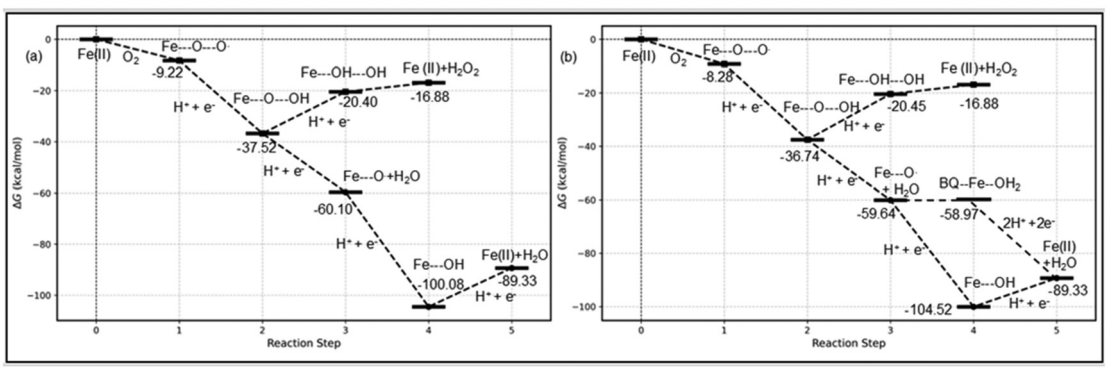

Fig. 5 Free energy profiles for H_2O and H_2O_2 formation with the (a) unsubstituted catalyst Fe(Sal) and (b) hydroquinone-substituted catalyst Fe(Sal-H_2Q), illustrating the effect of hydroquinone substitution on the reaction thermodynamics. Fe(III)–O can oxidize the H_2Q to BQ, and an alternative pathway is also viable.

Table 1 %H_2O_2 values obtained from RRDE measurements for Fe(Sal) and Fe(Sal-H_2Q) in an aqueous medium

Catalyst	pH	i_D (μA)	i_R (μA)	n
Fe(Sal)	4	29.09	0.052	3.95
Fe(Sal-H_2Q)	4	23.28	0.020	3.97
Fe(Sal)	5	29.4	0.001	3.99
Fe(Sal-H_2Q)	5	21.52	0.100	3.88

formation for both catalysts. This trend supports the experimental observations, in which water was observed as the major product with Fe(Sal-H_2Q) as well as Fe(Sal).

For Fe(Sal), the H_2O_2 formation pathway involves two energetically uphill steps, whereas the H_2O formation pathway requires overcoming only a single uphill step. The multiple positive ΔG increments in the H_2O_2 pathway highlight its relative thermodynamic disadvantage compared to the more straightforward H_2O pathway. Similarly, for Fe(Sal-H_2Q), the H_2O

pathway is thermodynamically favored over H_2O_2 formation, with a similar trend observed in the Gibbs free energy profile. Interestingly, the final net reaction Gibbs free energies (overall thermodynamics of the catalytic cycle) of both products, *i.e.*, H_2O and H_2O_2, are nearly identical for both Fe(Sal) and Fe(Sal-H_2Q), indicating that the overall thermodynamic driving force for product formation is independent of the covalent attachment of the H_2Q group. This observation suggests that the intrinsic thermodynamic stability of the products governs their favorability, rather than structural variations in the catalysts.

3. Conclusions

Thus, the current study demonstrates a reversal in the reactivity of the EPTM BQ/H_2Q covalently attached to Fe(Sal), for which the rate of the ORR is significantly hampered. The observation holds true for the ORR in non-aqueous and aqueous media. Spectroscopic and mechanistic investigations are underway to understand the origin of this detrimental reactivity.

4. Experimental section

Electrochemical measurements

All the measurements were performed in a three-electrode system using a CHI 7044E potentiostat. Non-aqueous Ag^+/Ag and a Pt wire were used as the pseudoreference and counter electrodes for homogeneous electrochemistry. Glassy carbon was used as a working electrode in all the experiments and polished after each scan. For anaerobic CV experiments, solutions were degassed by bubbling N_2 through the solvent for 30 min. In CV experiments in which O_2 was present, O_2 gas was purged into the glass cell containing solutions of the electrocatalyst stirred at 300 rpm for 20 min prior to data collection. Ferrocene was added to the solution at the end of each experiment, and a cyclic voltammetry scan was recorded to measure this potential to calibrate the Ag^+/Ag potentials with regard to $Fc^{+/0}$. All cyclic voltammetry experiments were conducted at a scan rate of 50 mV s^{-1}.

RRDE (rotating ring disk electrode) analysis

To study the selectivity of the catalyst in an aqueous medium, RRDE analysis was carried out using a CHI 7044E bi-potentiostat. The number of electrons (n) involved in the reaction and the amount of H_2O_2 generated during the ORR (oxygen reduction reaction) could be calculated from RRDE. The rotating ring disk electrode assembly comprised a rotating glassy carbon (GC) disk electrode with an area of 0.2 cm^2 and a platinum ring electrode (BAT SOL Equipment and Technology) with a collection efficiency (N) of 0.15. Ag/AgCl (saturated KCl) and Pt wire were used as the reference and counter electrode, respectively.

Preparation of the electrode. 1 mM catalyst was dispersed in 5 mL DCM and sonicated. 50 μL of this solution was drop-cast on the glassy carbon disk electrode for RRDE. After air drying, the electrode was rinsed with chloroform, ethanol, and water. Data were collected in air-saturated 100 mM phosphate buffer solutions (0.1 M Na_2HPO_4 and 0.1 M NaCl), and the pH was adjusted to pH 4 or 5 using phosphoric acid.

Conflicts of interest

There are no conflicts to declare.

Data availability

Supporting data is available in the supplementary information (SI). Supplementary information is available. See DOI: **https://doi.org/10.1039/d5dt01227a**.

Acknowledgements

B. M. acknowledges an IIT Gandhinagar internal grant and SERB-SRG (SRG/2022/001736) for funding; A. I. S. acknowledges IIT Gandhinagar for a fellowship. A. M. and Sanyam thank PARAM Ananta for the computational resources. Sanyam thanks CSIR for the fellowship.

References

1 S. Dey, B. Mondal, S. Chatterjee, A. Rana, S. Amanullah and A. Dey, *Nat. Rev. Chem.*, 2017, **1**, 0098.
2 Y. He, S. Liu, C. Priest, Q. Shi and G. Wu, *Chem. Soc. Rev.*, 2020, **49**, 3484–3524.
3 A. C. Brezny, S. I. Johnson, S. Raugei and J. M. Mayer, *J. Am. Chem. Soc.*, 2020, **142**, 4108–4113.
4 X. Li, H. Lei, L. Xie, N. Wang, W. Zhang and R. Cao, *Acc. Chem. Res.*, 2022, **55**, 878–892.
5 P. Mondol and C. J. Barile, *ACS Appl. Energy Mater.*, 2021, **4**, 9611–9617.
6 L. Wang, M. Gennari, F. G. Cantú Reinhard, J. Gutierrez, A. Morozan, C. Philouze, S. Demeshko, V. Artero, F. Meyer, S. P. de Visser and C. Duboc, *J. Am. Chem. Soc.*, 2019, **141**, 8244–8253.
7 R. Zhang and J. J. Warren, *ChemSusChem*, 2021, **14**, 293–302.
8 A. G. Reid and C. W. Machan, *J. Am. Chem. Soc.*, 2023, **145**, 2013–2027.
9 S. L. Hooe, E. N. Cook, A. G. Reid and C. W. Machan, *Chem. Sci.*, 2021, **12**, 9733–9741.
10 C. W. Anson and S. S. Stahl, *J. Am. Chem. Soc.*, 2017, **139**, 18472–18475.
11 S. V. Obisesan, C. Rose, B. H. Farnum and C. R. Goldsmith, *J. Am. Chem. Soc.*, 2022, **144**, 22826–22830.
12 S. V. Obisesan, M. Parvin, M. Tao, E. Ramos, A. C. Saunders, B. H. Farnum and C. R. Goldsmith, *Inorg. Chem.*, 2024, **63**, 14126–14141.
13 A. Singha, A. Mondal, A. Nayek, S. G. Dey and A. Dey, *J. Am. Chem. Soc.*, 2020, **142**, 21810–21828.

14 S. Dinda, A. I. Siddiqui, S. Behera and B. Mondal, *ACS Catal.*, 2023, **13**, 12643–12647.
15 E. N. Cook, S. L. Hooe, D. A. Dickie and C. W. Machan, *Inorg. Chem.*, 2022, **61**, 8387–8392.
16 S. Fukuzumi, W. Nam, X. Lu, Y. M. Lee and M. Sankaralingam, *Inorg. Chem.*, 2020, **59**, 18010–18017.
17 G. Tei, T. Tamaki, T. Hayashi, K. Nakajima, A. Sakai, S. Yotsuhashi and T. Ogawa, *Eur. J. Inorg. Chem.*, 2017, **2017**, 3229–3232.
18 C. T. Carver, B. D. Matson and J. M. Mayer, *J. Am. Chem. Soc.*, 2012, **134**, 5444–5447.
19 J. B. Gordon, A. C. Vilbert, I. M. Dimucci, S. N. MacMillan, K. M. Lancaster, P. Moënne-Loccoz and D. P. Goldberg, *J. Am. Chem. Soc.*, 2019, **141**, 17533–17547.
20 X. P. Zhang, A. Chandra, Y. M. Lee, R. Cao, K. Ray and W. Nam, *Chem. Soc. Rev.*, 2021, **50**, 4804–4811.
21 D. Chen and A. E. Martell, *Inorg. Chem.*, 1987, **26**, 1026–1030.
22 B. W. Purse, L. H. Tran, J. Piera, B. Åkermark and J. E. Bäckvall, *Chem. Eur. J*, 2008, **14**, 7500–7503.
23 R. Bonetto, R. Altieri, M. Tagliapietra, A. Barbon, M. Bonchio, M. Robert and A. Sartorel, *ChemSusChem*, 2020, **13**, 4111–4120.
24 P. D. Astudillo, D. P. Valencia, M. A. González-Fuentes, B. R. Díaz-Sánchez, C. Frontana and F. J. González, *Electrochim. Acta*, 2012, **81**, 197–204.
25 S. V. Obisesan, C. Rose, B. H. Farnum and C. R. Goldsmith, *J. Am. Chem. Soc.*, 2022, **144**, 22826–22830.
26 M. J. Frisch, G. W. Trucks, H. B. Schlegel, G. E. Scuseria, M. A. Robb, J. R. Chesseman, G. Scalmani, V. P. Barone, B. Mennucci, G. A. Petersson and H. Nakatsuji, Inc., Wallingford CT, 2009, **121**, 150–166.
27 N. Kerru, L. Gummidi, S. V. H. S. Bhaskaruni, S. N. Maddila, P. Singh and S. B. Jonnalagadda, *Sci. Rep.*, 2019, **9**, 1–17.